

# Organic magnetic-field effect examined in frequency domain and time domain

F. Wang<sup>a</sup>, R. Lin<sup>a</sup>, K. A. Hutchinson<sup>b</sup>, J. Rybicki<sup>a</sup>, and M. Wohlgenannt<sup>a</sup>

<sup>a</sup>Department of Physics and Astronomy, Optical Science and Technology Center, University of Iowa, Iowa City, IA-52242;

<sup>b</sup>Department of Electrical and Computer Engineering, University of Iowa, Iowa City, IA-52242

## ABSTRACT

Recent work has shown that weak applied magnetic fields of several tens of mT can lead to a change of several percent in the (photo)conductivity of organic semiconductor devices. However, it remains to be determined whether the applied magnetic field modifies the (photo)carrier density, their mobility or both. We use magnetic-field-dependent time-of-flight spectroscopy to disentangle these two possibilities. We find evidence that the magnetic field leads to a decrease in the photocarrier time-of-flight. We also examine organic magnetoresistive devices in the frequency domain to complete the characterization of the time-dependent field-effect response.

**Keywords:** Spintronics, organic semiconductor, organic magnetoresistance, photoconductivity, time of flight, frequency dependence

## 1. INTRODUCTION

Measurable effects due to small magnetic fields (tens of mT) were initially observed in (bio)chemical processes (Ref.<sup>1</sup> and refs. therein). An important example of a system that was studied is the primary reaction in photosynthesis.<sup>2</sup> A technologically important system involving photoexcitations is photoconductivity in organic semiconductor devices, which shows promise for solar energy production. Several studies of the steady-state photocurrent have revealed that it increases by several percent in an applied field of several tens of mT.<sup>3-5</sup> The following mechanism is usually employed to explain this observation: photoexcitation leads to the formation of an initially pure singlet radical pair (a.k.a. polaron pair), but triplet character develops due to hyperfine coupling. Assuming that the back-transfer reaction is different for singlet and triplet pairs, the charge separation efficiency will be affected by applied magnetic fields comparable to the hyperfine coupling strength.<sup>3,4</sup> Consequently, the number of free photocarriers becomes a function of the applied magnetic field.

Recent studies of the organic magnetoresistive (OMAR) effect (Ref.<sup>6-11</sup>) have revealed a new facet of magnetic field effects: the conductivity in organic semiconductor thin film devices, such as those used for organic light-emitting diodes (OLEDs), is also influenced by small applied magnetic fields. Fig. 1 shows typical magnetic-field effect traces for Alq<sub>3</sub> OMAR devices (see experimental section). The left inset shows the OMAR traces plotted over a smaller magnetic-field range showing that the most pronounced dependence of the current on the magnetic field occurs at fields well below 100 mT. Possible explanations for the organic magnetoresistive effect are more subtle than those for photoconductivity, since any intermediate pair states that may form during the conduction process are formed in a spin-independent manner. Indeed, the mechanism that causes this effect is presently strongly debated. Among the models proposed are the bipolaron model<sup>12</sup> and the polaron-triplet scattering mechanism<sup>9</sup> that lead to a magnetic field dependent mobility. Other models where the mobility is field-independent have also been proposed.<sup>7,8,11</sup> The possibility of a magnetic field effect on the mobility raises an interesting question: is the measured magnetic field effect on the steady-state photocurrent due to a change in carrier generation efficiency, or is it rather caused by a magnetic field effect on the carrier mobility? In this paper, we attempt to shed light on this question by studying time-resolved magnetic-field effect responses. Since the carrier time-of-flight is inversely proportional to the mobility, we can test for a magnetic-field dependent mobility by measuring the time-of-flight with and without magnetic field. We performed such experiments on an

---

Further author information: (Send correspondence to M. Wohlgenannt): E-mail: markus-wohlgenannt@uiowa.edu, Telephone: 1 319 353 1974

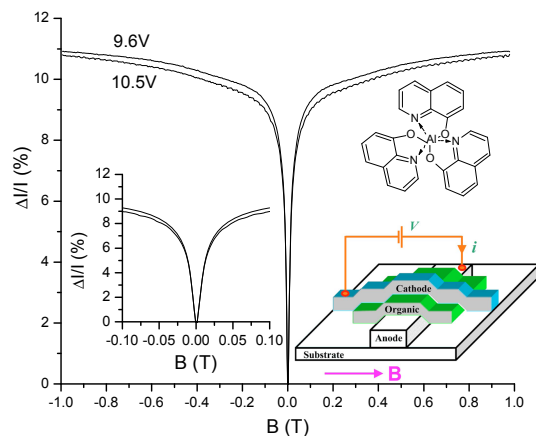


Figure 1. Typical magnetic-field effect traces for Alq<sub>3</sub> OMAR devices. The insets show the OMAR traces plotted over a smaller magnetic-field range, the Alq<sub>3</sub> molecular structure and the schematic OMAR device structure.

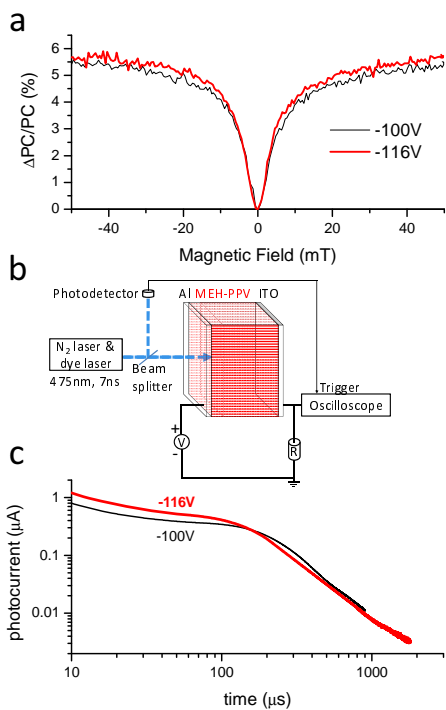


Figure 2. a) Magnetic field effect on the continuous wave photocurrent vs. magnetic field for two different reverse biases. b) Schematic drawing of the photocurrent time of flight setup. c) Time-resolved photocurrent for two different reverse biases.

organic photoconductive device based on a representative organic semiconductor, specifically poly[2-methoxy-5-(2-ethylhexyloxy)-1,4-phenylene-vinylene] (MEH-PPV). We will also examine the frequency-dependent response of OMAR devices as a second method of studying time-dependent magnetic-field effect responses. Our goal in these latter experiments is to examine a possible correlation between majority and minority carrier mobility and the OMAR response. For example, if OMAR is related to a magnetic-field dependent recombination of electron-hole pairs<sup>7</sup> we should find that the minority carrier mobility determines the frequency-resolved OMAR response, since the minority carrier mobility limits the electron-hole pair recombination rate.

## 2. EXPERIMENTS

Our devices for the time of flight measurement were fabricated on indium-tin-oxide (ITO) covered glass slides. The MEH-PPV polymer (American Dye Sources, used as received) film was deposited by drop casting from a 10 mg/ml toluene solution by slow evaporation in a solvent-rich environment resulting in a 2.9  $\mu\text{m}$  thick film. The residual solvent was removed by baking inside a glove box for 2 hours at 80  $^{\circ}\text{C}$ . Finally a semi-transparent, 20 nm thick Al top electrode was deposited by thermal evaporation in high vacuum. The devices were operated in dynamic vacuum at room-temperature.

The photocarrier time-of-flight traces were measured as follows (Fig. 2 b): A ThermoLaserScience 337-i model nitrogen pulsed laser was used for pumping a Lasertechnik Berlin UDL 100 dye laser. The output (475 nm, 7ns, 40  $\mu\text{J}$ /pulse) was focused onto the 0.5x1 mm<sup>2</sup> device area through the semi-transparent Al electrode. The time-resolved photocurrent was sensed using a 1kOhm resistor and recorded on a LeCroy LT 372 digital oscilloscope. We used the oscilloscope-internal averaging function to improve signal-to-noise. We employed a modulation type technique for the magnetic-field dependent time-of-flight measurements. A repeating series of traces was recorded with magnetic field on, off, off, on. This sequence, rather than the simpler on, off sequence was chosen to minimize the effect of temporal sample drift. The fractional change in time-resolved photocurrent was averaged over approximately 50 sequences to achieve a satisfactory signal-to-noise ratio. For comparison, we also measured the magnetic field effect on the continuous wave photocurrent in the same device (Fig. 2 a). For this measurement, we used an Ar<sup>+</sup> ion laser at 476.5 nm, adjusting the power until the magnitude of the steady state photocurrent equals  $\approx 1\mu\text{A}$ , a value typical for the photocurrent time-of-flight experiment.

Our frequency dependence measurements use OMAR devices with a relatively small device area (0.12x0.12 mm<sup>2</sup>) fabricated on Si/SiO substrates. The substrates were washed in several solvents using an ultrasonic cleaner and handled in a class 1000 clean-room. The bottom electrode for our organic sandwich devices was a 120  $\mu\text{m}$  wide, 20 nm thick Au electrode fabricated by e-beam evaporation through a shadow mask. A 2nm thick Cr adhesion layer was fabricated by e-beam evaporation prior to the Au deposition. A poly(3,4- ethylenedioxythiophene) poly(styrenesulfonate) (PEDOT:PSS, referred to as simply PEDOT from now on) layer ( $\approx 100$  nm) functioning as the hole-injecting electrode (anode in Fig. 1 inset) was deposited on top of the Au electrode by spin-coating. All subsequent steps were performed inside a glove box or the glove box integrated vacuum deposition chamber. As the organic semiconductor layer, a 50 nm thick Alq<sub>3</sub> (tris-(8-hydroxyquinoline) aluminum) layer was fabricated by thermal evaporation in high vacuum at a rate of 0.1 nm/s. Then a 120  $\mu\text{m}$  wide, 30 nm thick Ca top electrode covered by 30 nm of Al was deposited by electron beam evaporation through a shadow mask at a rate of 0.1nm/s. Ca is commonly used as an electron-injecting material (cathode in Fig. 1 inset) due to its small work function. The relatively small device area allows us to use a small electromagnet, which can be driven at higher frequencies. For the AC magnet we used a Ferrite coil driven by a function generator. In our measurements we use a constant applied voltage,  $V$ , and measures the changes,  $\Delta I$  in the device current,  $I$ . We also performed AC impedance and capacitance frequency measurement to allow correlation of the measured OMAR response to parameters such as the majority and minority carrier mobility. In these measurements we use a function generator as the AC source and a lock-in amplifier as the measurement unit.

## 3. DISCUSSION

### 3.1 Magnetic field effect on Time of flight measurement

The time-of-flight experiment involves photogeneration of a packet of charge carriers (initially confined to within the light absorption length of  $\approx 100$  nm) by illumination with the laser pulse. The drift of the carriers under an external bias to the collecting electrode results in the time-dependent photocurrent. The transit time  $\tau$  of the carriers is related to the carrier mobility  $\mu$  via the relation  $\mu = d/\tau E$ , where  $d$  is the film thickness and  $E$  the external bias field. We used reverse bias and this corresponds to drift of the holes, which are the species with larger mobility in MEH-PPV. Fig. 2 c shows the time-resolved photocurrent (photocarrier time-of-flight experiment) for two different reverse biases. The most important feature of the time-of-flight data is the shoulder that is visible in the data around 100  $\mu\text{s}$ , which defines the characteristic carrier time-of-flight. The log-log plot reveals a clear shoulder that separates data with a small exponent at small times, and a larger exponent at larger times. Such behavior is typical of time-of-flight traces in dispersive materials.

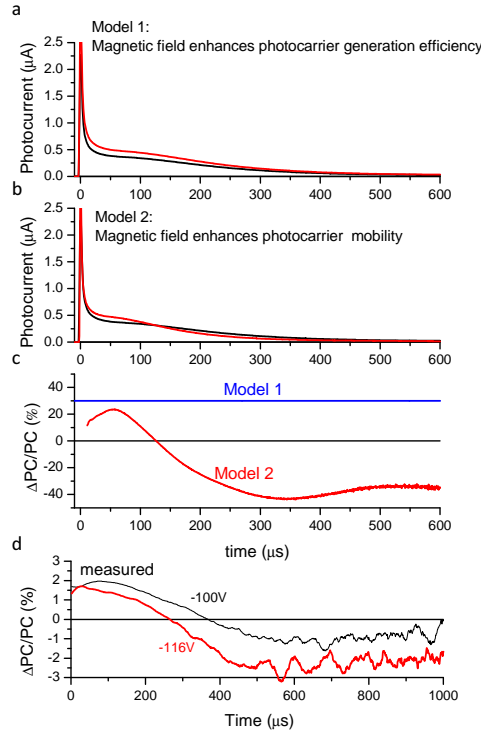


Figure 3. Magnetic field effect on the time-resolved photocurrent. a) Hypothesized scenario that the magnetic field affects the carrier generation efficiency (referred to as Model 1), b) Hypothesized scenario that the magnetic field affects carrier mobility (Model 2). c) Simulated magnetic field effects on the time-resolved photocurrent based on Model 1 and Model 2. d) Measured traces for two different reverse biases.

Several theories<sup>13, 14</sup> have been developed to account for this observation. An early model was developed by Scher and Montroll.<sup>13</sup> This model does not provide a quantitatively accurate description of dispersive transport in polymer films. However, it is sufficient for our purposes, since we are mainly interested in explaining the effect of a small perturbation on the transit time, and not in obtaining a quantitative model for the transit time itself. We will use this model to analyze the magnetic-field dependent time-of-flight traces to be discussed below. The reader is referred to Ref.<sup>14</sup> for more accurate models.

The Scher-Montroll model states that the shoulder occurs at the typical carrier transit time,  $\tau$ , and gives the following relation for the photocurrent time-dependence:

$$PC = \frac{\alpha Q}{2\tau} \left[ \left( \frac{t}{\tau} \right)^{-1+\alpha}, \left( \frac{t}{\tau} \right)^{-1-\alpha} \right] \text{ for } t < \tau, t > \tau, \quad (1)$$

where  $0 < \alpha < 1$  is a parameter that quantifies how dispersive the transport is, and  $Q$  is the total charge, i.e. the time-integral over the photocurrent. The time of flight traces in Fig. 2 c, are fitted with the Scher-Montroll expression, yielding  $\tau = 161\mu s$ ,  $\alpha = 0.95$  and  $\tau = 115\mu s$ ,  $\alpha = 0.85$  for -100 V and -116 V bias, respectively.

One of the main goal of this work is to examine the effect of an applied magnetic field on the photocarrier time-of-flight traces. In particular, our TOF experiments aim to determine whether the applied magnetic field modifies the photocarrier generation efficiency or their mobility, or both. For this purpose we first discuss the qualitative nature of the signals we would expect in these two cases. We examine two models (Fig. 3 a and b): In Model 1 the magnetic field enhances the photocarrier generation efficiency, leading to a magnetic field-induced

change in the total charge  $Q$ , but the mobility (and therefore transit time) remain unaffected; In the complement of Model 1, which we refer to as Model 2, the magnetic field enhances the photocarrier mobility, which leads to a change in carrier transit time.

To illustrate these two models, we perform an analysis using one of the experimental time-of-flight traces for zero field (Fig. 3 c, this time plotted on linear scales) for the simulations. We simulate the action of the magnetic field as follows: Since carrier photogeneration occurs on a nanosecond time-scale,<sup>1</sup> a change in  $Q$  by Model 1 corresponds to an instantaneous change in the photocarrier generation efficiency and should therefore result in a flat, i.e. time-independent fractional enhancement of the photocurrent. This expectation is displayed Fig. 3 a) where we simply multiplied the measured photocurrent trace by a constant to yield the simulated TOF trace in an applied B-field. Fig. 3 c) shows that this corresponds to a time-independent fractional enhancement of the photocurrent. For Model 2, however, we assume that the magnetic field increases the photocarrier mobility, which decreases the carrier transit time  $\tau$ . To simulate this we shrank the time scale of the zero-field data by a constant, and also multiply the photocurrent scale by the same constant to simulate the increased mobility that leads to a larger photocurrent. This yielded the expected high-field data, see Fig. 3 b). We then calculate the fractional change  $\Delta PC/PC$  between simulated high-field data and the zero-field data. The resulting curve is shown as Model 2 in Fig. 3 c). We see that the qualitative predictions of the two models are characteristically different. The curve for model 2 shows a zero crossing, whereas model 1 leads to a time-independent response.

Now we compare the model predictions to the experimentally measured data. Fig. 3 d) shows the magnetic field effect on the time of flight traces for two different reverse biases. The time-dependent  $\Delta PC/PC$  traces are very similar to our model 2 simulation. Therefore, they can only be understood when analyzed using the scenario that the photocarriers also experience an enhanced mobility in the applied magnetic field. As a result of the enhanced mobility, the photocarrier transit times will be reduced and the photocurrent will consequently decay faster, resulting in a smaller current at large times, and correspondingly, larger current at smaller times.

We also fitted our time-resolved traces in Fig. 3 d) with the Scher-Montroll theory. The best agreement between simulation and actual data is achieved with a 1.4% (1.4%) decrease in  $\tau$  and 0.4% (0.15%) increase in  $Q$  for -100V (-116V) bias.

### 3.2 Frequency dependence of magnetoresistance response

Fig. 4 a) shows the frequency dependent magnetoconductance response,  $\Delta I/\Delta I(0)$  of an Alq<sub>3</sub> OMAR device to an applied AC magnetic field of frequency,  $f$ . Defining the limit frequency  $f_{lim}$  as the frequency where the response has dropped to a value of  $1/e$  times that for  $f = 0$ , we find  $f_{lim} \approx 10$  kHz, roughly independent of device voltage. Now we move to the analysis of the obtained  $f_{lim}$ . What determines  $f_{lim}$ ? In principle, there are several time scales that could be of importance, such as the fundamental time scale of the spin-dependent interaction that causes OMAR, the majority (higher mobility) carrier transit time, the minority (lower mobility) carrier transit time, the detrapping time of carrier release from deep traps. The fundamental timescale of the reactions that causes OMAR, be it exciton or bipolaron formation, or scattering off triplet excitons, should be much too fast to cause a limit frequency of 10-100kHz. Time-of-flight measurements reported in the literature (see e.g. Ref.<sup>15</sup>) lead us to believe that the majority carrier transit time is also too short to be relevant at the 10kHz scale. However, it is quite reasonable to consider the minority carrier transit time as limiting the OMAR frequency response. This was indeed recently suggested by Wagemans et al.,<sup>16</sup> and we will follow a similar analysis.

Fig. 4 b) shows the measured AC admittance response to an AC voltage. The admittance is given by  $Y = dI/dV = G + i\omega C$ , where  $G$  is the conductance, and the out-of-phase part is the angular frequency times the capacitance  $C$ . The capacitance curve is the more interesting of the two. The capacitance starts out negative and then converges to the geometric capacitance. Although, to the best of our knowledge, the exact interpretation of the negative component to the capacitance is still being discussed, it is believed to be caused by a contribution of the minority carriers to the space charge stored inside the device.<sup>17,18</sup> Therefore, the transition frequency for the disappearance of the negative capacitance should be a measure of the minority carrier transit time. Wagemans et al. observe a correlation between the capacitive transition frequency and the OMAR limit frequency.<sup>16</sup> In our experiments, however, such a correlation is not evident, since the capacitive transition frequency is much lower than the OMAR limit frequency.

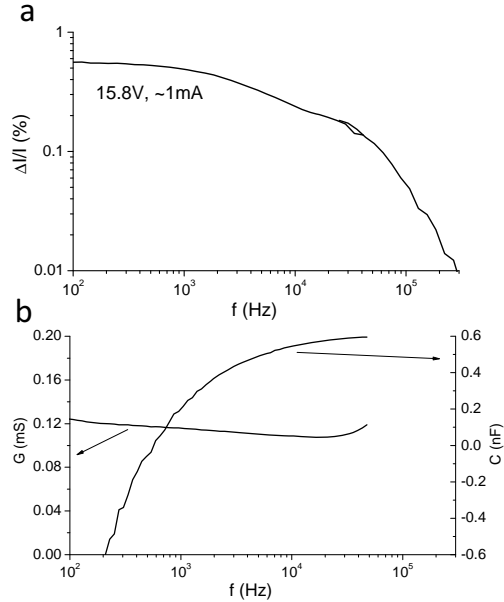


Figure 4. a) Magnetic field response  $\Delta I/I(0)$ , of the device current of an  $\text{Alq}_3$  OMAR device to an applied AC magnetic field of frequency  $f$ . b) Frequency-dependent conductance  $G$  and capacitance  $C$  at 15V.

#### 4. CONCLUSION

We showed that small magnetic fields can lead to a change in the photocarrier time-of-flight. This change reflects a change in mobility. Two mechanisms for a mobility sensitive to small magnetic fields have recently been proposed, the bipolaron<sup>12</sup> model and the triplet-polaron scattering mechanism.<sup>9</sup> Since scattering with triplets could occur only in the excitation region, whose thickness is negligible compared to the overall device thickness, our results are therefore consistent with the bipolaron mechanism, although a small contribution of the polaron-triplet mechanism is possible.

To complete our study of time-dependent magnetic-field effect response, we examined the frequency-dependent magnetoresistive response in  $\text{Alq}_3$  OMAR devices for frequencies up to 1MHz. The limit frequency of the  $\text{Alq}_3$  devices is about 10kHz. A possible explanation for the observed limit frequencies is the minority carrier transit time. We performed capacitance spectroscopy to further investigate this possibility. We observe negative capacitance at low frequencies, and positive capacitance at medium and high frequencies. According to some models, the transition between negative and positive capacitance is determined by the minority carrier transit time. In our measurements, we did however not find a clear correlation between the capacitive transition frequency and the OMAR limit frequency.

#### ACKNOWLEDGMENTS

This work was supported by Army MURI Grant No. W911NF-08-1-0317 and NSF Grant No. ECS 07-25280.

#### REFERENCES

1. Schulten, K., "Magnetic-field effects in chemistry and biology," *Festkörperprobleme-Adv. Solid State Phys.* **22**, 61 (1982).
2. Hoff, A. J., "Magnetic-field effects on photosynthetic reactions," *Q. Rev. Biophys.* **14**(4), 599 (1981).
3. Frankevich, E. L., Lymarev, A. A., Sokolik, I., Karasz, F. E., Blumstengel, S., Baughman, R. H., and Horhold, H. H., "Polaron-pair generation in poly(phenylene vinylenes)," *Phys. Rev. B* **46**(15), 9320 (1992).

4. Kalinowski, J., Szymtkowski, J. D., and Stampor, W., "Magnetic hyperfine modulation of charge photogeneration in solid films of alq(3)," *Chem. Phys. Lett.* **378**(3-4), 380 (2003).
5. Desai, P., Shakya, P., Kreouzis, T., and Gillin, W. P., "Magnetoresistance in organic light-emitting diode structures under illumination," *Phys. Rev. B* **76**(23), 235202 (2007).
6. Mermer, O., Veeraraghavan, G., Francis, T. L., Sheng, Y., Nguyen, D. T., Wohlgenannt, M., Kohler, A., Al-Suti, M. K., and Khan, M. S., "Large magnetoresistance in nonmagnetic pi-conjugated semiconductor thin film devices," *Phys. Rev. B* **72**(20), 205202 (2005).
7. Prigodin, V. N., Bergeson, J. D., Lincoln, D. M., and Epstein, A. J., "Anomalous room temperature magnetoresistance in organic semiconductors," *Synth. Met.* **156**(9-10), 757 (2006).
8. Hu, B. and Wu, Y., "Tuning magnetoresistance between positive and negative values in organic semiconductors," *Nat. Mater.* **6**(12), 985 (2007).
9. Desai, P., Shakya, P., Kreouzis, T., Gillin, W. P., Morley, N. A., and Gibbs, M. R. J., "Magnetoresistance and efficiency measurements of alq(3)-based oleds," *Phys. Rev. B* **75**(9), 094423 (2007).
10. Bloom, F. L., Wagemans, W., Kemerink, M., and Koopmans, B., "Separating positive and negative magnetoresistance in organic semiconductor devices," *Phys. Rev. Lett.* **99**(25), 257201 (2007).
11. Wang, F. J., Bassler, H., and Vardeny, Z. V., "Magnetic field effects in pi-conjugated polymer-fullerene blends: Evidence for multiple components," *Phys. Rev. Lett.* **101**(23), 236805 (2008).
12. Bobbert, P. A., Nguyen, T. D., van Oost, F. W. A., Koopmans, B., and Wohlgenannt, M., "Bipolaron mechanism for organic magnetoresistance," *Phys. Rev. Lett.* **99**(21), 216801 (2007).
13. Scher, H. and Montroll, E. W., "Anomalous transit-time dispersion in amorphous solids," *Phys. Rev. B* **12**(6), 2455 (1975).
14. Bassler, H., "Charge transport in disordered organic photoconductors - a monte-carlo simulation study," *Physica Status Solidi B-Basic Research* **175**(1), 15 (1993).
15. Redecker, M., Bradley, D. D. C., Inbasekaran, M., and Woo, E. P., "Nondispersive hole transport in an electroluminescent polyfluorene," *Appl. Phys. Lett.* **73**(11), 1565 (1998).
16. Wagemans, W., Janssen, P., van der Heijden, E. H. M., Kemerink, M., and Koopmans, B., "Frequency dependence of organic magnetoresistance," *Appl. Phys. Lett.* **97**, 123301 (2010).
17. Gommans, H. H. P., Kemerink, M., Andersson, G. G., and Pijper, R. M. T., "Charge transport and trapping in cs-doped poly(dialkoxy-p-phenylene vinylene) light-emitting diodes," *Phys. Rev. B* **69**(15), 155216 (2004).
18. Gommans, H. H. P., Kemerink, M., and Janssen, R. A. J., "Negative capacitances in low-mobility solids," *Phys. Rev. B* **72**(23), 235204 (2005).